Strength analysis of critical components of high-pressure fuel pump with hypocycloid drive

M. BAJERLEIN[iD], M. BOR, W. KARPIUK[iD], R. SMOLEC[iD], and M. SPADŁO[iD]

Poznan University of Technology, Faculty of Civil and Transport Engineering, Piotrowo 3, 61-138 Poznań, Poland

Abstract. Most high-pressure fuel pumps for compression-ignition engines manufactured today are cam driven. These pumps have numerous advantages, such as low energy consumption and limited production costs. However, a problem arising from the nature of the cam mechanism is an unfavorable distribution of forces in the camshaft-plunger-cylinder system of a delivery section. The authors have proposed an innovative pump design that eliminates most of the problems present in conventional solutions. The pump utilizes a gear-based hypocycloid drive. This paper focuses mainly on the strength analysis of the two critical components (countershaft and mount) of the subassembly under the highest load – simulations were carried out for different critical load states. The following procedure of estimating fatigue life was adopted for computations: the operational evolution of stresses will be systematized to the set of amplitude stresses and mean stresses by means of the "Rainflow" method. The results obtained in the work showed that the main factor determining change of stresses was the presence of clearances in the pump mechanism. It has been proved that the values of clearances have a negative influence on the power transmission in particular – their presence results in loads being carried by the countershaft and not by the support inter-operating with it. This may cause frictional wear of teeth, leading to the improper operation of the transmission. The analysis showed that the mount was designed correctly. This facilitates the use of less demanding constructional materials.

Key words: strength analysis, FEM, high-pressure pump, pump with hypocycloid drive, fuel injection systems.

1. Introduction, pump with hypocycloid drive

Modern fuel systems in compression-ignition engines facilitate fuel injection into the combustion chamber under a very high pressure, exceeding 250 MPa. Reaching such high values is necessary due to rigorous emission standards [1–3]. Increasing injection pressure makes it possible to reduce droplet diameters, which increases the total surface area of their evaporation, thereby improving the quality of the combustion process. High pressure also translates into a relatively short injection time, which allows the combustion engine to reach high power while maintaining adequate environmental parameters.

The pump, usually made with a single plunger or multiple plungers, is responsible for generating the correct fuel pressure. Most designs use a cam drive with a centrally situated drive shaft [4–6]. This type of construction is relatively inexpensive, which obviously is an advantage. However, these pumps have their flaws – one of the problems is the cam drive itself. In this type of solutions, there is an additional force component perpendicular to the longitudinal axis of the plunger [7, 8]. The occurrence of the so-called lateral forces in the plunger-cylinder system of a delivery section may result in the increased frictional resistance, which leads to a substantial limitation of the unit durability, particularly when fuels of inadequate quality or unconventional fuels are used [9–11].

Another problem is the need to use fuels of good quality. This is significant, because Diesel oil compressed in the pump simultaneously serves as a lubricant and coolant for the pump interior components. A change of the physicochemical properties of the fuel, e.g. the reduction of lubricity, increase of viscosity or density, may lead to the damage of precision friction pairs, which are the most important elements of a delivery section. Also, when there is too much water content in the fuel, corrosion may appear, manifesting as the presence of permanent inclusions which may lead to more rapid clogging of the fuel filter, and as a consequence, may also penetrate the area of the pump moving parts. Analogous phenomena occur when impurity content in the fuel is too high.

The analysis conducted by the authors of the existing solutions applied in high-pressure pumps demonstrated that none of the current designs are devoid of flaws. Flaws can be eliminated by introducing certain design changes, which will lead to improved reliability. The conducted assessment enabled the authors to propose an innovative pump drive that addresses the most important problems of high-pressure engine pumps – a hypocycloid mechanism was utilized to drive the plunger [12–14]. The concept of this mechanism was developed as early as in the 19th century. Nevertheless, it has not been applied in plunger pump solutions until now. Its most significant advantage is the absence of a lateral force acting on the plunger-cylinder surface, as well as a high stroke of the working element with respect to the overall dimensions of the pump.

Its operation is based on the application of a pair of gears, in which the larger gear has interior toothing, and the smaller gear has exterior toothing, where the ratio of the number of
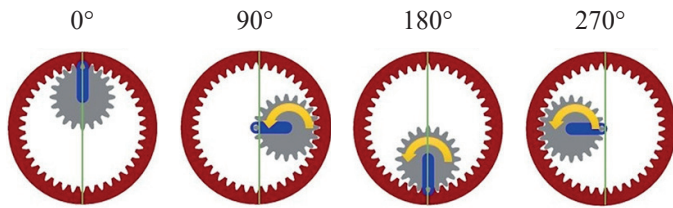
Fig. 1. Concept of the hypocycloid mechanism's operation

teeth is equal to 2. The gear with interior toothing is fastened to the body of the pump, while the smaller gear rolls over its circumference. In such a situation, a selected point on the circumference of the smaller gear, whose distance from the center of the gear is equal to half of the larger gear radius, performs reciprocating motion in a straight line (Fig. 1).

Using the above power transmission concept, the pump design was created from the ground up. This solution was patented [15]. In this scope, several variants were prepared, with 1 to 4 delivery sections. This article focuses on the simplest of these variants, based on one delivery section (Fig. 2).
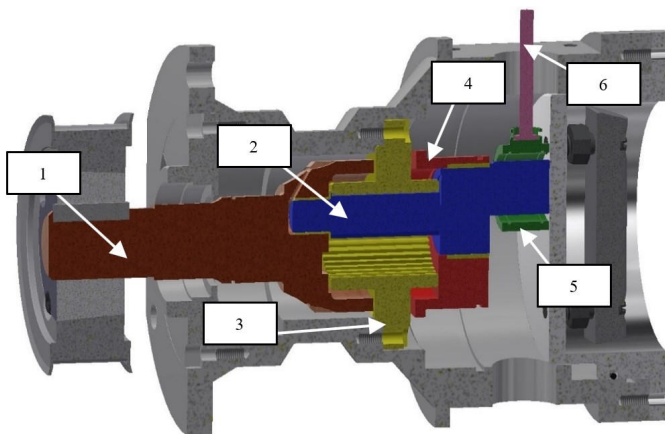

Fig. 2. Simplified model of hypocycloid pump presenting the most important components of the design: 1 – main shaft, 2 – countershaft, 3 – gear with interior toothing, 4 – support, 5 – mount, 6 – plunger

The design of the pump considers load variability – it means that the pump has been designed to increase the fatigue strength. Thus, the fatigue strength has been included during the analyses, considerations, and pump design. The pump has a main shaft (1) to which power is transmitted. A countershaft (2) is mounted in the main shaft in such a manner that mutual rotation of both components is possible. The countershaft, with the gear mounted on a part of it, rolls over the circumference of gear (3). Support (4) is a component that interacts with the countershaft from the side of the delivery section. The countershaft also inter-operates with the mount (5) via a bearing. The plunger (6) and its guiding element, situated so that it can slide within the cylinder of the delivery section, is fixed to this mount. The authors have given a detailed description of the design in [16–18]. What is noteworthy is that, due to the mechanism applied, this design makes it possible to completely eliminate lateral forces in the delivery section system. Moreover, the presented solution has two significant advantages. The first of them pertains to the pressure chamber of the delivery section. Through the application of a system of labyrinth seals, the flow is completely isolated from the crankcase, and the thick walls of both bodies also provide thermal insulation. Such a solution makes it possible to apply a separate lubrication system, which allows for pumping the fuels of poorer quality, including those characterized by high chemical aggression and high temperatures.

The second advantage is a very large stroke of the plunger, which makes it possible to employ the effect of gas desorption from the solution with nucleation of gas bubbles. This is an innovative solution tested at the Poznań University of Technology, involving the dissolution of exhaust gases in the fuel followed by the reversal of the phenomenon and release of this gas from the solution during its injection into the combustion chamber. The high-pressure pump, the delivery section of which is the site of gases dissolution in the fuel, is critical in this process. The desorption effect has been described in greater detail in [19–22]. It must be stressed, however, that the final pump design largely depends on the possibility of applying the aforementioned effect.

Creating this innovative design from scratch required diligent performance of individual stages of the prototype construction by the design team. Evaluation of the strength of the critical components of the selected pump was an important step – the goal of the article was to evaluate the strength of the pump countershaft and mount (Figs. 2; 2 and 5), which are part of the delivery section. They are among the components of the design under the greatest load. Performance of such an analysis enabled us to determine tolerable stresses in the components of the subassembly, which facilitated the correct selection of structural materials in the subsequent stages of the task. Phenomena occurring in the area of contact between the gears, e.g. the precise distribution of contact stresses, were not accounted for in detail in the discussion. The fact that torque was transmitted by the power transmission was considered.

The first component is the part of the pump responsible for power transmission – it connects the pump main shaft to the delivery section. A point selected on the radius of the countershaft gear travels along a curve called a hypocycloid. The second of the analyzed parts is mounted on the countershaft and is responsible for transmitting force directly to the pump plunger. For simulation purposes, it was accepted that this force is equal to 5300 N for the extreme loading case (fuel pressure 160 MPa). The mount consists of a ring (interlocking with the countershaft) and holder, in which the plunger is fastened. The plunger rests on the base of the holder during the discharge phase, and during the fuel suction phase, it is pulled downwards by a pin fixed in the holder's recess. Therefore, it can be assumed that the mount will carry the highest load during the fuel compression stroke. In order to estimate occurring forces, a FEM model of the component was made, loading states were determined for different clearance variants (none, 0.05 mm, and 0.1 mm) between parts, and strength computations of this component were carried out.

2. Methods

2.1. Numerical model. The numerical model was built based on three-dimensional, tetrahedral finite elements of the second order (Fig. 3), as described in [23–25]. This made it possible to obtain a good degree of fill of the geometry, particularly for complex shapes and edges [26, 27]. Basic parts of the pump mechanism were used to build the model. Computations omitted the pump covers due to the absence of forces acting on them and due to their significantly lower rigidity with respect to the pump body. Components such as rolling bearings, bolts, plunger, and ring seals were also omitted. The interactions of these components were represented by applying external loads or removing degrees of freedom and implementing the appropriate finite elements [28, 29].
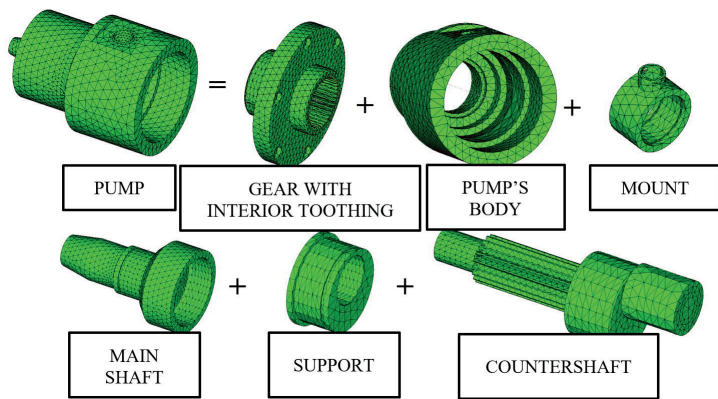

Fig. 3. Numerical components of the pump with mesh

2.2. Boundary conditions. The evolution of generated torque (supra-plunger force) as a function of the pump shaft position was adopted as the basis for computations. Load can be generated in two ways depending on the conventional action and reaction. In the first variant, rotation of the simulated main shaft of the pump can be blocked and supra-plunger force can be applied

for the given angular position of units. In the second variant, it is possible to block the simulated mount and apply torque to the main shaft. The first variant was selected in the conducted simulations, and force was applied at the base of the pump plunger. Loading cases are shown in Fig. 4 – for the left and right figure, the shaft only works under the bending force. For the middle figure, the shaft works under the bending force and the torsional force. Therefore, the middle figure shows a higher load condition. Due to the very low compressibility of fluid for the adopted forces, it was accepted that the start of the compression is also the instant at which the force reaches its maximum value (5300 N).

The angular position range of the shaft from 0° to 180° is characterized by the absence of supra-plunger force. Therefore, if small forces of inertia and friction in the nodes are omitted, it can be assumed that stresses for this loading period will be negligibly small. For the bottom extreme position, after closing of the inlet valve, due to the negligible compressibility of the fluid, the supra-plunger force reaches its maximum, equal to 5300 N. In this position, the mechanism transmits the maximum bending moment, and the torsional moment is equal to zero since $x = 0$. In this case, the top fibers of the mechanism are subjected to tension and the bottom fibers to compression. After the transition to the 270° position, these fibers are found on the plane intersecting the neutral axis, thus stresses reach a value equal to zero. In further motion, they change signs upon reaching the upper extreme point of stress. This cycle can be described as stress change cycle I.

Cycle II pertained to stress changes between 90° and 270°. Similarly, as previously assumed, no load will be present at the 90° position. Nevertheless, the loading state will be at maximum at the 270° position, i.e. bending and torsional moments reach maximum values, where the bending moment acts on fibers on which no forces acted at the 180° or 0° position (intersection with neutral axis).

Prior to the analysis, it is impossible to unequivocally determine which of the described situations is more demanding for the construction. Albeit it is true that a complex state of effort arising from the presence of bending and torsional moment is present at 270°. However, over the course of complete shaft
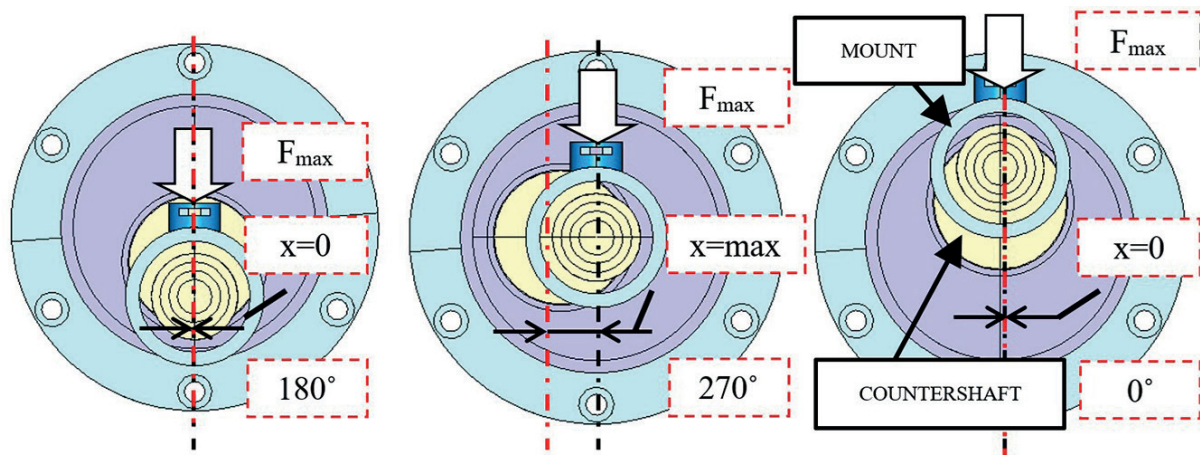

Fig. 4. Simulated extreme pump loading cases

rotation, stresses increase from zero (90°) to the maximum value. Meanwhile, between 180° and 0°, a change occurs from negative (minimum) stresses to maximum stresses, which may induce fatigue effects earlier. Everything depends on the proportion between the bending and torsional moments (and therefore also on the radius "x") and on the structure resistance to these inputs.

2.3. Inferencing rules. The pump unit predominantly works within the fatigue range, which means that stresses periodically increase to their maximum value and then decrease for every revolution of the drive shaft. The determinant of strength is therefore the structure work within the range of the fatigue limit, i.e. for an infinite number of loading cycles. The following procedure of estimating fatigue life was adopted for computations: the operational evolution of stresses will be systematized to the set of amplitude stresses σ_a and mean stresses σ_m by means of the "Rainflow" method [30, 31]. Amplitude and mean stresses are determined based on maximum and minimum stresses, according to the formulas:

$$\sigma_a = \frac{\sigma_{MAX} - \sigma_{MIN}}{2}, \quad \sigma_m = \frac{\sigma_{MAX} + \sigma_{MIN}}{2} \tag{1}$$

σ_{MAX} and σ_{MIN} are determined from FEM analysis.

The "Rainflow" method is currently the most common technique for processing random loads, since it presents well stress changes that occur in metals [32, 33].

"Rainflow" is used to determine loading cycles, which are all spans forming closed hysteresis loops and loading half-cycles that do not form such loops [34, 35]. In this way, it becomes possible to relate the stochastic evolution of stresses to fatigue curves plotted under determinate conditions on strength testers. The effects of the procedure implementation are illustrated in Fig. 5.

Obtained stresses are then confronted with two-parameter fatigue curves, where parameter N, determining the number of cycles until the occurrence of fatigue fracture, is linked to stresses σ_a and σ_m through surface equations of the general form $N = f(\sigma_a, \sigma_m)$. Charts of this type include, e.g. the Goodman-Smith diagram or Haigh diagram.

Amplitude stresses plotted on the chart should not exceed the lines delimiting the fatigue limit. Otherwise, there is a risk of premature fatigue cracking. If these curves are not available, which is unfortunately a rather common problem, particularly for "exotic" materials, it is possible to perform reduction of asymmetrical stress cycles to oscillatory cycles using selected models. Popular models include the Goodman [38], Soderberg [38], Gerber [38], Morrow [38] and Smith-Watson-Topper models [39]. This article presents cycles reduced by using the Smith-Watson-Topper method [39, 40] (recommended by [40]), in which:

$$\sigma_{SWT} = \sqrt{(\sigma_a + \sigma_m) \cdot \sigma_a} \tag{2}$$

where: σ_a – cycle amplitude stresses, σ_m – cycle mean stresses. It is then possible to evaluate fatigue strength using a single-parameter fatigue characteristic, e.g. Wohler curve, or by comparing stresses with constants determining the fatigue limit, e.g. for tension (k_r). Huber-Mises-Hencky [36, 41] stresses were applied to evaluate the influence of the stress tensor multidimensionality on the material strength. Since this is the preliminary stage of simulations, more refined methods, e.g. based on the critical plane (described in, e.g. [16, 17, 39, 42]), were not applied. However, to increase the certainty of considerations, a sign change of H-M-H stresses was applied depending on whether compression or tension was more dominant.

3. Results and discussion

This subsection presents the results of the strength analysis. As mentioned earlier, computations were carried out for three positions of the main shaft: 0°, 180° and 270°. Three analyses were performed in each position of the main shaft, for different clearance cases – zero, minimum and maximum. The zero-clearance case is the reference variant that enables evaluation of the effects of the presence of clearance in the pump. The second case concerns the situation when clearances assume minimum values (from the bottom interval), and the third case when clearances assume maximum values (from the top interval). All cases are illustrated in Figs. 6–11, and precise values are given in Tables 1 and 2. In Table 2, for the mount, only
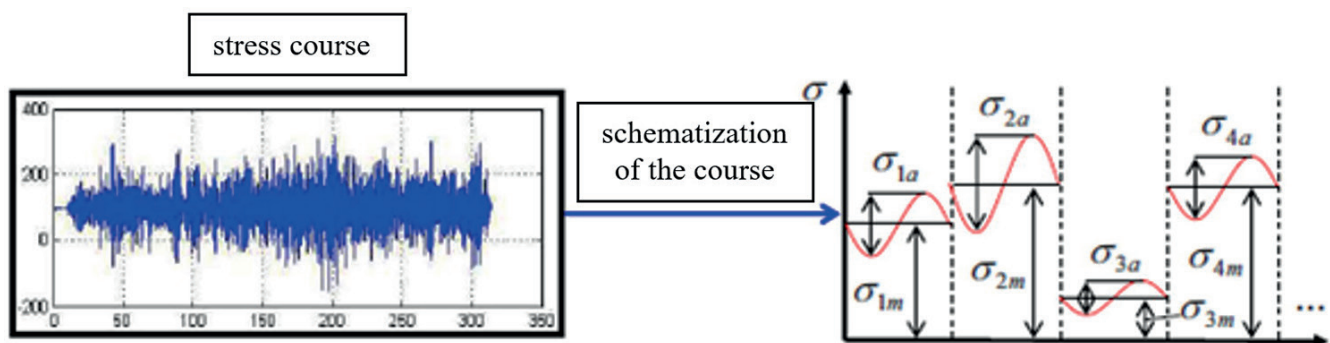

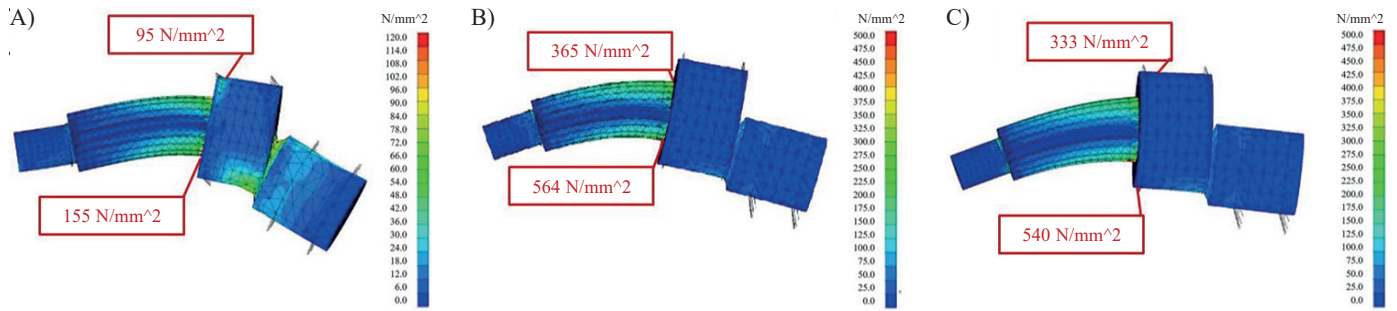Fig. 5. Effect of processing random load evolutions using schematization methods [36, 37]

Fig. 6. Countershaft, isolines of Huber-Mises-Hencky stresses for displacement of mesh nodes at a scale of 150:1 – case of position at BDC (180°) for zero clearance (A), minimum clearance (B) and maximum clearance (C)
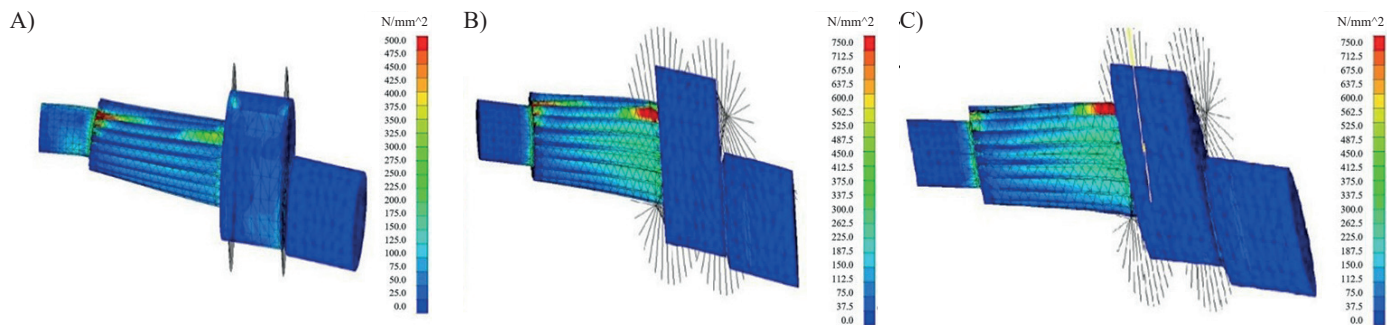

Fig. 7. Countershaft, isolines of Huber-Mises-Hencky stresses for displacement of mesh nodes at a scale of 50:1 – case of shaft position at 270° for zero clearance (A), minimum clearance (B) and maximum clearance (C)
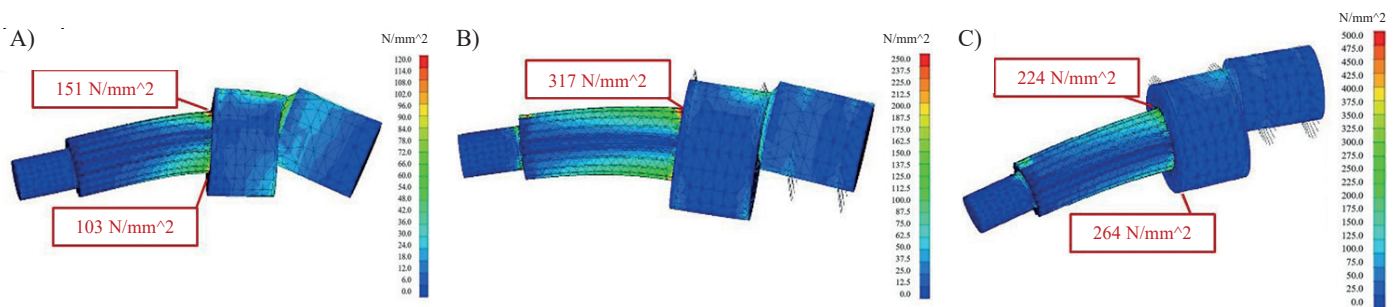

Fig. 8. Countershaft, isolines of Huber-Mises-Hencky stresses for displacement of mesh nodes at a scale of 150:1 – case of shaft position at 0° for zero clearance (A), minimum clearance (B) and maximum clearance (C)
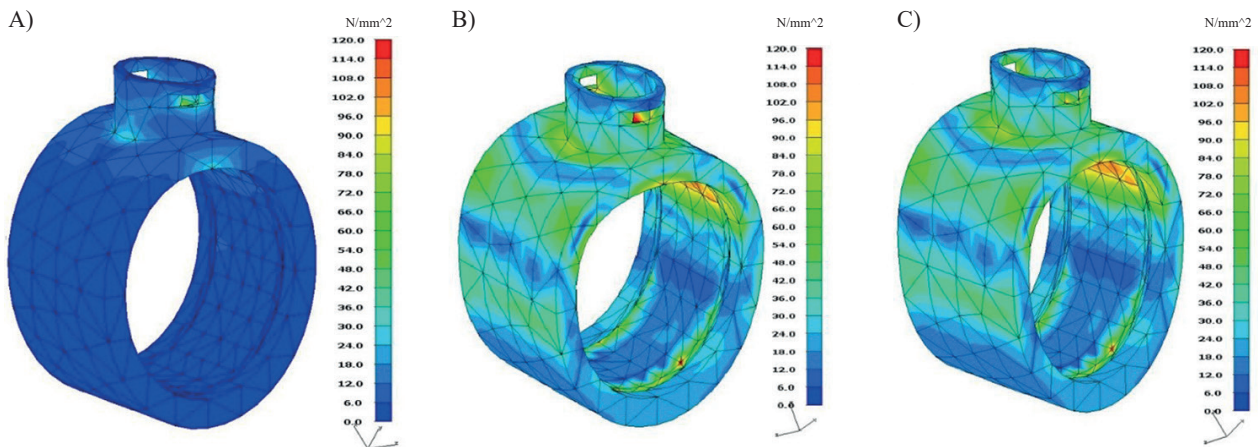

Fig. 9. Mount, isolines of Huber-Mises-Hencky stresses for displacement of mesh nodes at a scale of 150:1 – case of position at BDC (180º) for zero clearance (A), minimum clearance (B) and maximum clearance (C)

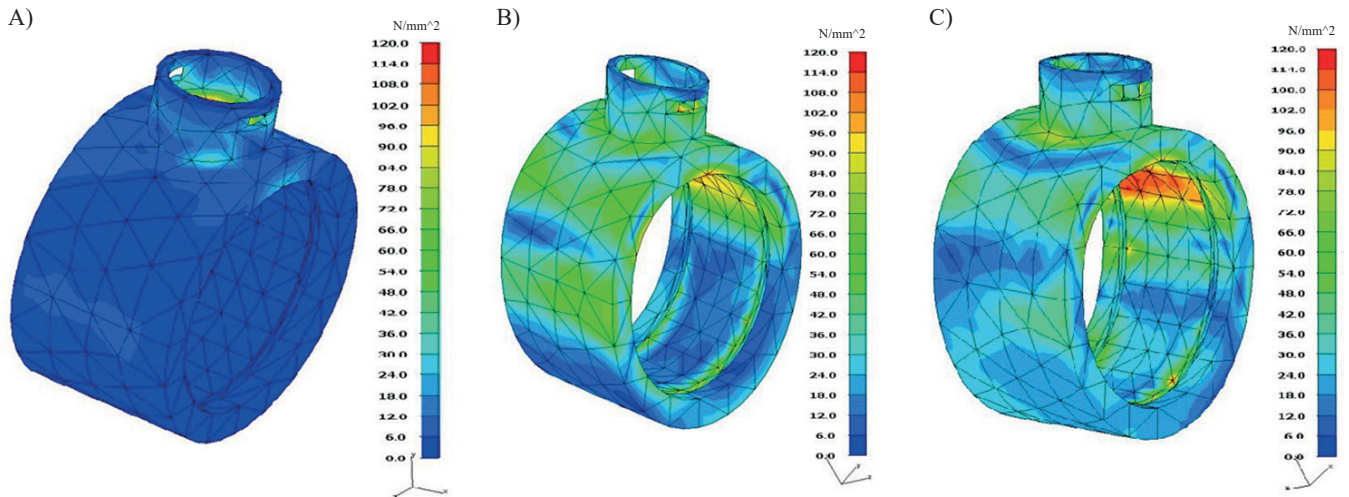M. Bajerlein, M. Bor, W. Karpiuk, R. Smolec, and M. Spadło

Fig. 10. Mount, isolines of Huber-Mises-Hencky stresses for displacement of mesh nodes at a scale of 100:1 – case of shaft position at 270°
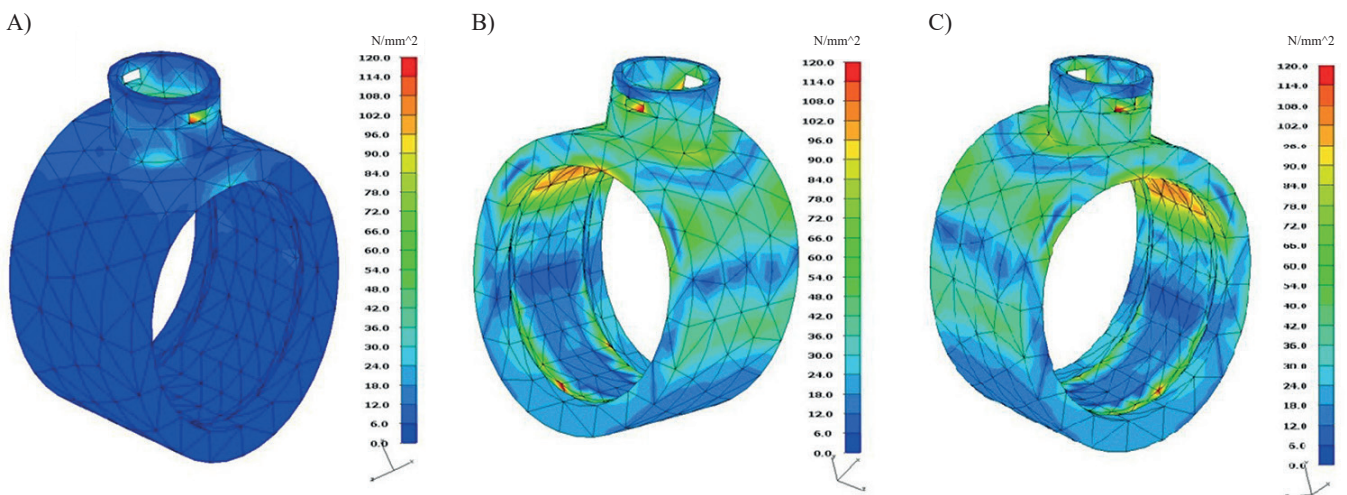for zero clearance (A), minimum clearance (B) and maximum clearance (C)

Fig. 11. Mount, isolines of Huber-Mises-Hencky stresses for displacement of mesh nodes at a scale of 150:1 – case of shaft position at 0° for
zero clearance (A), minimum clearance (B) and maximum clearance (C)

Table 1
Stresses of countershaft for individual cases

Case	Cycle I				
	$\sigma_{MIN(90°)}$	$\sigma_{MAX(270°)}$	σ_{a_II}	σ_{m_II}	σ_{SWT_II}
No clearance	151 MPa	155 MPa	129 MPa	75 MPa	141 MPa
Minimum clearance	317 MPa	−564 MPa	440 MPa	−123 MPa	497 MPa
Maximum clearance	324 MPa	−540 MPa	432 MPa	108 MPa	483 MPa
	Cycle II				
No clearance	0 MPa	450 MPa	225 MPa	225 MPa	318 MPa
Minimum clearance	0 MPa	734 MPa	367 MPa	367 MPa	519 MPa
Maximum clearance	0 MPa	767 MPa	384 MPa	384 MPa	543 MPa

Table 2
Stresses of mount for individual cases

Case	Cycle II				
	$\sigma_{MIN(90°)}$	$\sigma_{MAX(270°)}$	σ_{a_II}	σ_{m_II}	σ_{SWT_II}
No clearance	0 MPa	36 MPa	18 MPa	18 MPa	25 MPa
Minimum clearance	0 MPa	102 MPa	51 MPa	51 MPa	72 MPa
Maximum clearance	0 MPa	120 MPa	60 MPa	60 MPa	84 MPa

stresses which reached a significant value from the perspective of strength are presented, the minimum threshold of which was accepted to be 50 MPa – that is why the previously mentioned cycle I is not found in the presented results.

The conducted analyses were used to determine substitute stresses using the previously described Smith-Watson-Topper method. The Huber-Mises-Hencky method was applied in the analysis of multiaxial fatigue loads, therefore, the given dependency should be fulfilled for the considered element:

$$stresses_{SWT} < tensile\ strenght \cdot safety\ factor. \qquad (3)$$

Tensile strength values can be obtained in [43]. The presented reference case without clearance was an idealized case for which the minimum tensile strength of the countershaft material should be no less than 211 MPa. For the mount, this value should be no less than 28 MPa. However, there are clearances in the actual structure of the mechanism, which increase stresses substantially and change their distribution. The change of the clearance level from minimum to maximum by itself did not cause a significant change in the stresses, and the primary factor determining the change of stress values was the presence of the clearance. The risk of fatigue damage will therefore accelerate exponentially, according to the scheme: wear causes clearances that accelerate wear. For maximum clearance, tensile strength was determined to be 483 MPa for the shaft and 84 MPa for the mount, which constitute, 2.3-fold and 3-fold values with respect to the case of no clearance, respectively.

Table 1 shows that for countershaft, the change in stress between the minimum and maximum clearance is not a considerable one (up to 5%). Negative values mean that there has been a change in the direction of stresses relative to the state where stresses have been assigned positive values. This means that when the shaft turned 180°, the sign of stresses changed for the upper and lower layers of the shaft material (tension turned into compression – similar to bending). In the case of mount (Table 2), the changes amount to a maximum of 15%. Based on the analysis of fatigue parameters (σ_{SWT_II}), it should also be stated that the effect of clearance is not unequivocal. For the countershaft, for cycle I, maximum values (497 MPa) were obtained for minimum clearances. However, for cycle II, maximum values (543 MPa) were obtained for maximum clearances. Therefore, the minimum clearance in cycle I is preferable because cycle II, due to its nature, is more demanding for

the system. It should also be remembered that in the process of using the pump, increasing the clearance will increase the stress.

The presence of clearances results in considerably increased stresses. At the same time, no significant differences in stress levels were observed between minimum and maximum clearances. Clearances have an adverse effect on power transmissions. The pinion begins to carry loads that should be carried by the support. This is particularly visible in the comparison in Fig. 12.
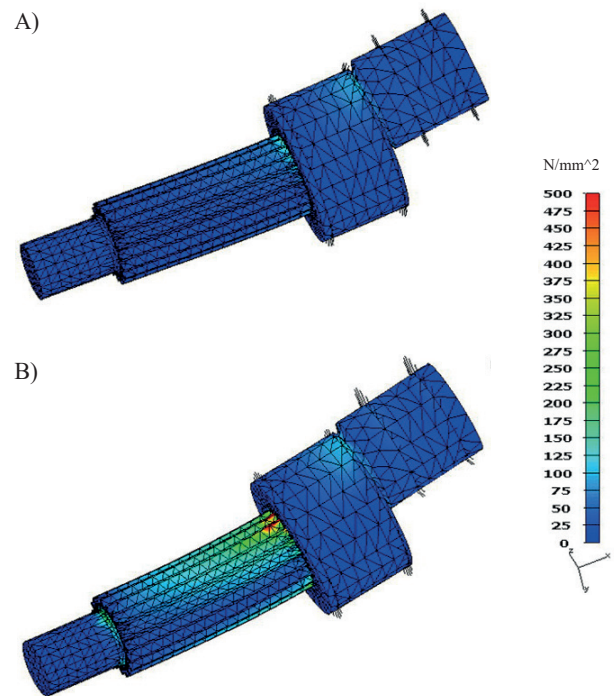

Fig. 12. Influence of the presence of clearance on levels of stresses in the pinion (A – without clearance, B – with maximum clearance)

The teeth of the pinion are pushed into the intertooth spaces of the gear. This phenomenon will cause additional frictional wear, resulting in the deformation of teeth, and consequently, inadequate work of the entire transmission. Moreover, the shaft transmits the bending moment to a greater extent – and this effect is nontrivial, as shown in Fig. 13 (the same scale of stresses was applied).
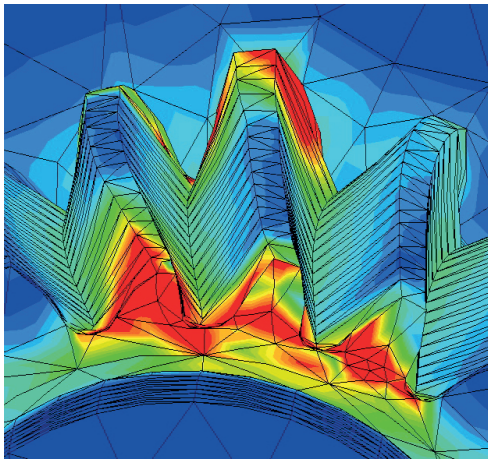
Fig. 13. Character of interoperation between teeth in the transmission

Care for proper surface processing of interlocking surfaces for this pair and for maintaining the proper dimensional tolerances is critical for ensuring the possibility of the long-term pump operation.

It can be stated that, in terms of strength, the mount has been designed properly – maximum stresses are low and reach the value of 84 MPa. In relation to this, low-strength steel may be applied, and stress concentrations in the mount, where the plunger pushes down on the base, are also the consequence of the applied method of load application (concentrated force) and will not occur in reality (Fig. 14).
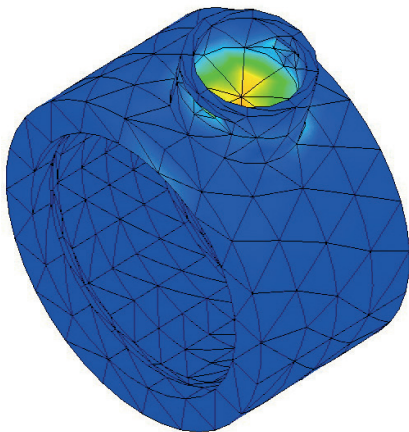

Fig. 14. Numerical stress concentrations in the mount

In structural terms, it is necessary to introduce an additional support for the mount, protecting against the possibility of buckling (Fig. 15). In the current solution, the risk that this effect will occur is high. Slight displacement of the force vector will induce an additional bending moment. The resistance to loads of this type of the node joining the plunger base with the mount is drastically low. The radius of the base is very small; therefore, the moment will reach high values under constant force.
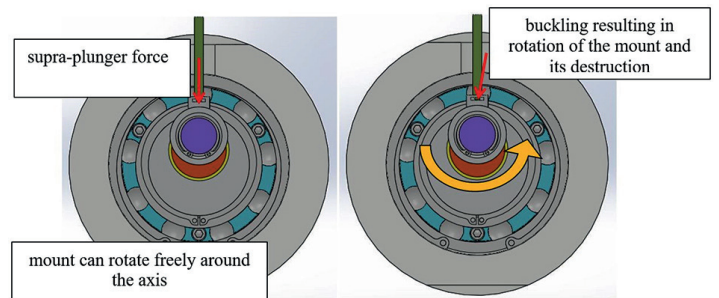

Fig. 15. Buckling mechanism in mount area

Based on simulation results, the authors proposed design changes to the mount, involving tapering of the mount and the application of a sliding support in a pump cover that works with the mount. The idea of these changes is presented in Fig. 16.
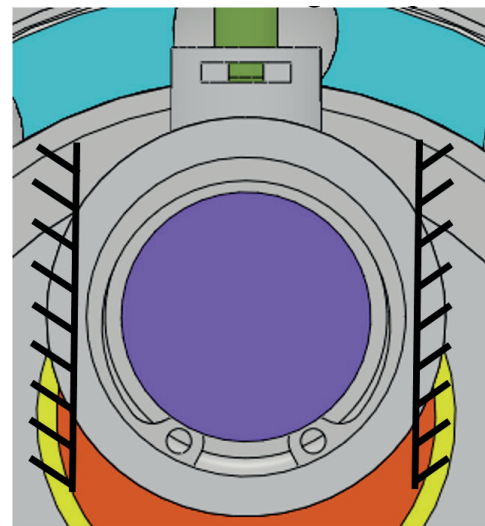

Fig. 16. Design change to mount

4. Conclusions

In this article, strength analysis of the two critical components under the greatest load in the original high-pressure pump intended for application in compression-ignition engines was undertaken. The authors proposed an innovative pump drive, briefly presented in the first part of the article, working based on an applied hypocycloid power transmission. The application of such a mechanism makes it possible to considerably reduce the flaws present in classical solutions, the operation of which is based on cam drives. Performance of analysis described in the article made it possible to determine tolerable stresses. It allowed us to select constructional materials in the next stages of making a prototype.

FEM modeling and simulations made it possible to draw conclusions of a practical nature. They can be summarized in the following points:

1. The main factor determining the change of stresses was the presence of clearances in the transmission. The conducted analysis unequivocally demonstrates that the risk of fatigue damage will increase as clearances increase, which will cause even greater wear as a result. At maximum clearances, the tensile strength of the countershaft is 483 MPa, and of the mount 84 MPa. This constitutes, a value 2.3 times and 3 times greater than for the case of no clearance, respectively. This conclusion indicates the need to significantly minimize the clearances during the manufacturing of pump components.

2. Clearances values indicated in the article have a negative influence on the power transmission in particular – their presence results in loads being carried by the countershaft and not by the support inter-operating with it. This may cause the frictional wear of teeth, leading to improper operation of the transmission.

3. For the power transmission to work properly, it is indispensable to perform the appropriate surface processing of the components and to maintain the appropriate dimensional tolerances – this will enable long-term, reliable operation of the subassembly.

4. In terms of strength, the mount was designed correctly – maximum stresses reach a value of 84 MPa. This allows for the use of less demanding constructional materials. However, it proved necessary to introduce an additional support for the mount – the risk of buckling occurring in this component was estimated to be at a high level.

In summary, the conducted analyses largely contributed to a better design – the guidelines concerning constructional materials were applied in the pump prototype. Changes in the design resulting from the analysis were also implemented in the final design of the pump with hypocycloid drive.

REFERENCES

[1] A. Jaworski, H. Kuszewski, A. Ustrzycki, K. Balawender, K. Lejda, and P. Woś, "Analysis of the repeatability of the exhaust pollutants emission research results for cold and hot starts under controlled driving cycle conditions", *Environ. Sci. Pollut. Res.* 25(18), 17862–17877 (2018).

[2] H. Kokota, H. Kosaka, K. Tsujimura, and T. Kamimoto, "Fast burning and reduced soot formation via ultra-high pressure diesel fuel injection", *SAE [Tech. Pap.]* 910225, 1–9 (1991).

[3] A. Minato, T. Tanaka, and T. Nishimura, "Investigation of pre-mixed lean diesel combustion with ultra-high-pressure injection", *SAE [Tech. Pap.]* 2005-01-0914, 1–9 (2005).

[4] A. Bąkowski and L. Radziszewski, "Determining selected diesel engine combustion descriptors based on the analysis of the coefficient of variation of in-chamber pressure", *Bull. Pol. Ac.: Tech*. 63(2), 457–464 (2015).

[5] A. Ferrari, P. Pizzo, and R. Vitali, "Development and validation procedure of a 1D predictive model for simulation of a common rail fuel injection system controlled with a fuel metering valve", *SAE Int. J. Engines* 11(4), 401–422 (2018).

[6] R.D. Lockett and M. Jeshani, "An experimental investigation into the effect of hydrodynamic cavitation on diesel", *Int. J. Engine Res.* 14(6), 606–621 (2013).

[7] Y. Bai, Q. Lan, L. Fan, X. Ma, and H. Liu "Investigation on the fuel injection stability of high pressure common rail system for diesel engines", *Int. J. Engine Res.* 1468087419856981 (2019). doi: 10.1177/1468087419856981

[8] A. Ferrari and P. Pizzo, "Fully predictive common rail fuel injection apparatus model and its application to global system dynamics analyses", *Int. J. Engine Res.* 18(3), 273–290 (2016).

[9] O. Armas, C. Mata, and S. Martínez-Martínez, "Effect of an ethanol–diesel blend on a common-rail injection system", *Int. J. Engine Res.* 13(5), 417–428 (2012).

[10] Z. Stelmasiak, "Uniformity of Diesel oil dosage in dual fuel engines", *Eksploat. i Niezawodn.* 16(3), 491–495 (2014).

[11] J. Szczepaniak and M. Spadło "The issue of fatigue evaluation of agricultural machines shown in a multi-role unit", *Agric. Eng.* 4(139), 411–420 (2012).

[12] E.S. Aziz, "Enhanced hypocycloid gear mechanism for internal combustion engine applications", *J. Mech. Des.* 138, 1–9 (2016).

[13] M.A. El Bahloul, E.S Aziz, and C. Chassapis, "Mechanical efficiency prediction methodology of the hypocycloid gear mechanism for internal combustion engine application", *Int. J. Interact. Des. Manuf.* 13(1), 221–233 (2019).

[14] D.M. Ruch, F.J. Fronczak, and N.H. Beachley "Design of a Modified Hypocycloid Engine", *SAE [Tech. Pap.]* 911810: 73–90 (1991).

[15] W. Karpiuk, R. Smolec, and T. Borowczyk, "High-pressure engine-feeding pump", Patent No. PL232500, (2018) [in Polish].

[16] M. Bor, T. Borowczyk, M. Idzior, W. Karpiuk, and R. Smolec, "Analysis of hypocycloid drive application in a high-pressure fuel pump", *MATEC Web Conf.* 118, 00020 (2017).

[17] M. Bor, T. Borowczyk, W. Karpiuk, and R. Smolec, "Modeling of selected design characteristics of cam and hypocycloidal drives of high-pressure fuel pumps", *Adv. Sci. Technol. Res. J.* 12(2), 128–136 (2018).

[18] M. Bor, T. Borowczyk, W. Karpiuk, M. Spadlo, and R. Smolec, "Concept of a pump for diesel engines fuel supply using hypocyloid drive", *IOP Conf. Series: Materials Science and Engineering* 421, 042034 (2018).

[19] W. Kozak, "Forming the parameters of diesel engines injection", Poznan Univeristy of Technology Publishing House, Poznań, (2008) [in Polish].

[20] W. Kozak, M. Bajerlein, and J. Markowski, "Verification of the concept of spray mechanism assisted with air dissolved in diesel oil", *Combust. Engines*, 1/2006(124), 21–37 (2006).

[21] W. Kozak, M. Bajerlein, and J. Markowski, "The application of gas dissolved in fuel with a view to improve the mechanism of spraying" *Combust. Engines*, 1/2005 (120), 4–18 (2005).

[22] J. Merkisz, W. Kozak, M. Bajerlein, and J. Markowski, "The influence of exhaust gases dissolved in diesel oil on fuel spray particulary parameters", *SAE [Tech. Pap.],* 2007-01-0488, 1–9 (2007).

[23] P. Lonkwic, P. Różyło, and H. Dębski, "Numerical and experimental analysis of the progressive gear body with the use of finite-element method", *Eksploat. i Niezawodn.* 17 (4), 544–550 (2015).

M. Bajerlein, M. Bor, W. Karpiuk, R. Smolec, and M. Spadło

[24] M. Nowak, "Improved aeroelastic design through structural optimization", *Bull. Pol. Ac.: Tech.* 60(2), 237–240 (2012).

[25] W. Ostapski, A. Aromiński, and S. Dowkontt "The vibration of prototype aircraft propeller speed reduction unit – test bench and FEM numerical simulation study". *Bull. Pol. Ac.: Tech.* 62(4), 861–873 (2014).

[26] S. Kocańda and J. Szala, "Basics of fatigue calculations", Scientific Publishers PWN, Warsaw, (1997) [in Polish].

[27] L. Rybarska-Rusinek "On evaluation of influence coefficients for edge and intermediate boundary elements in 3D problems involving strong field concentrations", *Bull. Pol. Ac.: Tech.* 67(1), 69–76 (2019).

[28] M.W. Brown and K.J. Miller "A theory for fatigue failure under multiaxial stress-strain conditions", *Proceedings of the Institution of Mechanical Engineers,* 187, 69–71 (1973).

[29] T.M. Huber, "Proper work of deformation as a measure of material effort", *Technical Journal* Lviv, 22, (1904), [in Polish].

[30] I. Rychlik, "A new definition of the rainflow cycle counting method", *Int. J. Fatigue* 9(2), 119–121 (1987).

[31] M. Tinsdale, P. Price, and R. Chen, "The impact of biodiesel on particle number, size and mass emissions from a Euro4 diesel vehicle", *SAE Int. J. Engines* 3(1), 597–608 (2010).

[32] P. Johannesson, "On rainflow cycles and the distribution of the number of interval crossings by a Markov chain", *Probab. Eng. Mech.* 17, 123–130 (2002).

[33] M. Mrzygłód "Multi-constrained topology optimization using constant criterion surface algorithm", *Bull. Pol. Ac.: Tech.* 60(2), 229–236 (2012).

[34] C. Lalanne "Mechanical vibration and shock analysis", Vol. 2, Wiley-ISTE, London, (2009).

[35] M.A. Meggiolaro and J.T. Castro, "An improved multiaxial rainflow algorithm for non-proportional stress or strain histories – Part I: Enclosing surface methods", *Int. J. Fatigue* 42, 217–226 (2012).

[36] J. Badur, M. Bryk, P. Ziółkowski, D. Sławiński, P. Ziółkowski, S. Kornet, and M. Stajnke "On a comparison of Huber-Mises-Hencky with Burzynski Pecherski equivalent stresses for glass body during nonstationary thermal load", *AIP Conference Proceedings*, 1822(020002) (2017).

[37] M. Spadło, "Adaptation of fatigue analysis methods in the aspect of load stochastics for agricultural machines", Poznań, Doctoral thesis, (2014) [in Polish].

[38] Y.-L. Lee, J. Pan, R. Hathaway, and M. Barkey, "Fatigue testing and analysis. Theory and practice", Elsevier Butterworth-Heinemann, Burlington, 2005.

[39] T. Łagoda and M. Kurek, "Multiaxial random fatigue of machine elements", *Scientific Journal of the Military University of Land Forces*, 4(174), 104–117 (2014).

[40] S.S. Manson and G.R. "Halford fatigue and durability of structural materials", ASM International (2006).

[41] D. Skibicki, "Fatigue criterion based on the huber-von mises-hencky criterion for non-proportional loadings", *Journal of Polish CIMAC*, 5(3), 177–186 (2010).

[42] N. Vasiraja and P. Nagaraj "The effect of material gradient on the static and dynamic response of layered functionally graded material plate using finite element method", *Bull. Pol. Ac.: Tech.* 67(4), 827–838 (2019).

[43] M.E. Niezgodziński and T.B. Niezgodziński, "Formulas, charts and strength tables", Scientific and Technical Publishers, Warsaw, (2013) [in Polish].